

Scattering State Theory for One-dimensional Floquet Lattices

Ren Zhang,¹ Xiao-Yu Ouyang,^{1,2} Xu-Dong Dai,¹ and Xi Dai^{1,*}

¹*New Cornerstone Science Laboratory, Department of Physics,*

The Hong Kong University of Science and Technology, Clear Water Bay, Kowloon 999077, Hong Kong, China

²*Division of Chemistry and Chemical Engineering, California Institute of Technology, Pasadena, CA 91125, USA*

We develop a Floquet transfer matrix method to solve scattering in extended 1D Floquet lattices, uncovering an underlying conjugate symplectic structure that enforces current conservation across sidebands. By engineering a spatial adiabatic boundary, we suppress multi-channel sideband interference, allowing us to establish a direct mapping between the bulk winding number C and a rigid shift in the transmission energy windows—quantified as $C\hbar\omega$. We further propose two experimental realizations: cold-atom Bragg scattering to directly verify the transmission shift, and surface-acoustic-wave-induced transport demonstrating the quantized zero-bias current plateau.

Introduction.—The most important feature of electronic states in a periodic potential is the formation of energy bands—an effect entirely absent in free space [1, 2]. As a result, the electronic spectrum develops “forbidden bands”, within which no electronic wave can propagate [3]. If the chemical potential lies within such a gap, the system becomes an insulator [4]. Thus, the emergence of forbidden bands serves as the most fundamental and direct manifestation of quantum-mechanical effects induced by spatial periodicity. An intriguing question then naturally arises: what happens if the potential becomes periodic in both space and time [5–7]? Do the forbidden bands survive under spatiotemporal modulation [8]? If not, what new signatures emerge in electronic transport for such a spatiotemporal periodic system [9]?

In this work, we try to answer the above questions by exploring a scattering problem on a one-dimensional potential which is periodic in both time and space. It is well established that the transmission behavior through a one-dimensional lattice is intimately linked to its band structure: transmission is non-zero within energy bands but vanishes in the band gaps. When the scattering potential possesses time periodicity, the problem is termed Floquet scattering [10]. The one-dimensional Floquet scattering problem has been explored in numerous previous studies, which have established basic theoretical frameworks [11–13]. However, existing investigations have largely focused on scattering from small-scale barriers—such as molecular junctions—leaving the problem of scattering in extended Floquet lattices in the thermodynamic limit relatively unexplored. Furthermore, current theoretical frameworks often lack a comprehensive treatment of the fundamental mathematical structures that govern transport in these extended systems. In this work, we develop a framework for reformulating the Schrödinger equation into a set of first-order spatial equations in terms of frequency-component vectors with spatial derivatives. We then integrate this approach into a Floquet transfer matrix method, uncovering the inherent symplectic structure of the Floquet system [14–16]. Utilizing this framework, we develop a scattering theory for Floquet lattices that yields several key physical insights.

Furthermore, much like ordinary Bloch bands in a static periodic potential, Floquet–Bloch bands can also be classified according to their topological properties. A systematic classification framework was developed about a decade ago. In particular, for one-dimensional systems, Floquet–Bloch bands fall into a \mathbb{Z} -class characterized by an integer winding number [17]. Physically, this winding number measures the non-adiabatic charge pumping induced by the time-periodic driving potential [18, 19]. Despite this theoretical understanding, how such charge pumping can be realized and experimentally detected in real physical systems remains unclear. This question will be another central focus of the present work. By solving a one-dimensional Floquet–Bloch tunneling problem, we demonstrate that the topological index of a Floquet–Bloch band can be extracted from the analysis of its tunneling rate, thereby providing a possible route toward future experimental identification.

Floquet transfer matrix and symplectic structure.—We consider a single particle in a one-dimensional potential $V(x, t)$ that is periodic in time with period $\tau = 2\pi/\omega$. The Schrödinger equation (set $m = 1/2, \hbar = 1$) is

$$i \frac{\partial \psi}{\partial t} = \left[-\frac{\partial^2}{\partial x^2} + V(x, t) \right] \psi. \quad (1)$$

Using the Floquet ansatz $\psi(x, t) = e^{-i\epsilon t} \sum_n \phi_n(x) e^{-in\omega t}$ [6], where ϵ is the quasi-energy, and expanding the potential as $V(x, t) = \sum_n V_n(x) e^{-in\omega t}$, we obtain a second-order equation for the N -dimensional Fourier-component vector $\Phi = [\dots, \phi_{-1}, \phi_0, \phi_1, \dots]^T$ (frequency cutoff N) [11]:

$$\frac{d^2 \Phi}{dx^2} = M(x) \Phi, \quad M_{mn} = -(\epsilon + n\omega) \delta_{mn} + V_{m-n}(x). \quad (2)$$

Defining the wave-function vector (WFV) $Y = [\Phi^T, \partial_x \Phi^T]^T$ of dimension $2N$, Eq. (2) becomes a first-order equation

$$\frac{d}{dx} Y(x) = G(x) Y(x), \quad G(x) = \begin{pmatrix} 0 & I \\ M(x) & 0 \end{pmatrix}. \quad (3)$$

Then, the evolution of the WVF is governed by the *Floquet transfer matrix*

$$F(x_2, x_1) = \mathcal{X} \exp \left[\int_{x_1}^{x_2} G(x) dx \right] \quad (4)$$

where \mathcal{X} denotes spatial path-ordering. It gives $Y(x_2) = F(x_2, x_1)Y(x_1)$. Therefore a Floquet state at any spatial point is completely described by its WVF, allowing scattering problems to be formulated entirely in the frequency domain.

Using the WVF, we find that the time-averaged probability current $\overline{j(x)} = -i\frac{1}{\tau} \int_0^\tau dt [\psi^* \partial_x \psi - \partial_x \psi^* \psi]$ can be reformulated into the following form

$$\overline{j(x)} = -i Y^\dagger(x) J Y(x), \quad J = \begin{pmatrix} 0 & I_N \\ -I_N & 0 \end{pmatrix}. \quad (5)$$

The conservation of current implies that the Floquet transfer matrix F is *conjugate symplectic* (CSp) and conversely [20]:

$$\overline{j(x_1)} = \overline{j(x_2)} \Leftrightarrow F^\dagger J F = J. \quad (6)$$

The generator G in Eq. (4) satisfies the infinitesimal CSp condition $G^\dagger J + J G = 0$, which is equivalent to $\partial_x \overline{j(x)} = 0$. This CSp condition can be satisfied under any frequency cutoff with Symplectic integrator [14, 21].

When the potential is also spatially periodic with period d , i.e., $V(x+d, t+\tau) = V(x, t)$, diagonalization of a unit-cell transfer matrix $F(d, 0)$ yields Bloch and evanescent waves at a given quasi-energy. The CSp structure leads to two important spectral properties [21]:

1. Reciprocal eigenvalue pairing: For every $\lambda \in \sigma(F)$, one has $1/\lambda^* \in \sigma(F)$, where $\sigma(F)$ is the spectrum of F . Eigenvalues with $|\lambda| \neq 1$ come in conjugate-reciprocal pairs, describing left- and right-decaying evanescent waves, with N_E modes for each type; eigenvalues on the unit circle ($|\lambda| = 1$) are self-reciprocal and correspond to propagating Bloch waves (Fig. 1).

2. Current-balance: The numbers of Bloch-wave eigenvalues with positive and negative time-averaged current are equal, $N_+ = N_- = N_B$ [21, 22]. This balance is essential for constructing well-posed scattering problems.

Moreover, the eigenvectors of F obey an orthonormality and completeness relation adapted to the symplectic metric. For each eigenpair $(Y_\alpha, \lambda_\alpha)$ its reciprocal conjugate \bar{Y}_α (eigenvalue $1/\lambda_\alpha^*$) satisfies $\bar{Y}_\alpha^\dagger J Y_\alpha \neq 0$. Defining the dual vector

$$Y_\alpha^\dagger \equiv (\bar{Y}_\alpha^\dagger J Y_\alpha)^{-1} \bar{Y}_\alpha^\dagger J, \quad (7)$$

we obtain the orthonormal basis relations [21]

$$Y_\alpha^\dagger Y_\beta = \delta_{\alpha\beta}, \quad \sum_\alpha Y_\alpha Y_\alpha^\dagger = I_{2N}. \quad (8)$$

The Floquet transfer matrix formalism (Eq. (4)) and its conjugate symplectic structure (Eqs. (6)-(8)) provide

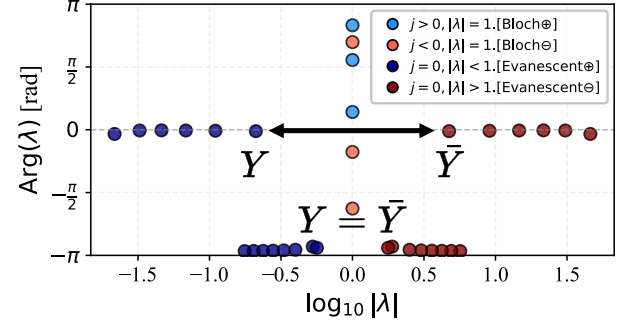


FIG. 1. Spectrum of a Floquet transfer matrix F . Dark blue (red) points represent left-decaying (right-decaying) evanescent waves; pale blue (red) points correspond to left- (right-) moving Bloch waves.

the complete framework for analyzing scattering between different Floquet lattices. This framework is our first key result. In the following sections we apply this machinery to two-region and three-region junctions, deriving general transmission/reflection matrices and, ultimately, a closed-form expression for the transmission matrix of an adiabatically graded interface.

Floquet Bragg Scattering— We study one-dimensional Bragg scattering between two semi-infinite Floquet lattices (Fig. 2a). An incident wave from the left lattice (Region A) propagates toward the right lattice (Region B). In Region B, the transmitted field consists of right-propagating Bloch waves and right-decaying waves, while in Region A, the reflected field consists of left-propagating Bloch waves and left-decaying waves.

For any Floquet lattice, we construct its Floquet transfer matrix F and obtain its spectrum $\sigma(F)$ with corresponding eigenstates. Based on the spectrum, eigenstates are grouped into right-propagating/decaying modes $\{Y_i\}_r$ and left-propagating/decaying modes $\{Y_i\}_l$. These states are arranged into matrices: $A_\oplus = [Y_{i_1}, \dots, Y_{i_N}]$ for $\{Y_i\}_r$ and $A_\ominus = [Y_{j_1}, \dots, Y_{j_N}]$ for $\{Y_i\}_l$, with evanescent modes listed first followed by Bloch modes (Fig. 2b). Similarly, for Region B we have B_\oplus and B_\ominus . From continuity of the wave function and its derivative, we have

$$A_\oplus + A_\ominus R_L = B_\oplus T_L, \quad B_\ominus + B_\oplus R_R = A_\ominus T_R. \quad (9)$$

Here, A_\oplus (A_\ominus) represents incident (reflected) waves, and B_\oplus (B_\ominus) represents transmitted (reflected) waves; all are $2N \times N$ matrices. R_L, R_R and T_L, T_R are reflection and transmission matrices.

The scattering process: the n th incident mode in A_\oplus generates the m th reflected mode in A_\ominus with amplitude $[R_L]_{mn}$, and the k th transmitted mode in B_\oplus with amplitude $[T_L]_{kn}$. Using orthonormality $A_\oplus^\dagger A_\oplus = I$ and $A_\oplus^\dagger A_\ominus = 0$, we derive

$$T_L = (A_\oplus^\dagger B_\oplus)^{-1}, \quad R_L = A_\ominus^\dagger B_\oplus (A_\oplus^\dagger B_\oplus)^{-1}. \quad (10)$$

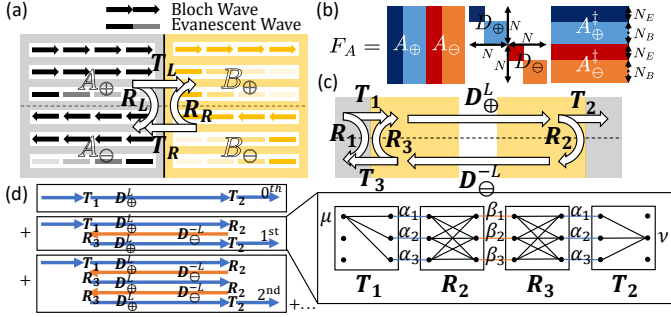


FIG. 2. (a) Schematic of the scattering between two semi-infinite regions A (left gray part) and B (right yellow part). (b) Diagonalization of Floquet transfer matrix. (c) Schematic of three-segment scattering. (d) Schematic of the loop and path expansions for the total transmission matrix in three-segment scattering.

Here, $A_{\oplus}^{\dagger} = [Y_1^{\dagger}, \dots, Y_N^{\dagger}]$ and $A_{\ominus}^{\dagger} = [Y_{N+1}^{\dagger}, \dots, Y_{2N}^{\dagger}]$. Thus, transmission and reflection matrices between Floquet lattices are extracted from the WFV of the Floquet transfer matrix. T_R and R_R are obtained similarly.

We next consider a three-segment scattering problem: a Floquet lattice sandwiched between two free-space regions (Fig. 2c). Free space is treated as a trivial Floquet lattice. Solving the Floquet transfer matrix for each segment yields Bloch and evanescent modes. Using the two-segment formalism (Eq. 10), we compute transmission and reflection matrices at both interfaces (T_i and R_j in Fig. 2c). Since evanescent modes decay exponentially for large lattice size $L \rightarrow \infty$, we introduce propagation matrices $D_{\oplus/\ominus} = \text{diag}[e^{ik_1 d}, \dots, e^{ik_{N_B} d}, 0, \dots, 0]$ for the central region, where $e^{ik_j d} = \lambda_j$ is the eigenvalue of the Bloch WFV, d is the lattice constant, and N_B is the number of Bloch modes.

Direct transmission through both interfaces gives the 0th order term $T_2 D_{\oplus}^L T_1$. Multiple reflections between interfaces yield higher-order terms $T_2 (D_{\oplus}^L R_3 D_{\ominus}^{-L} R_2)^n D_{\oplus}^L T_1$, with n round-trip reflections. Summing all paths gives the total transmission matrix

$$T = T_2 (1 - D_{\oplus}^L R_3 D_{\ominus}^{-L} R_2)^{-1} D_{\oplus}^L T_1. \quad (11)$$

The matrix element $T_{\mu\nu}$ accounts for all scattering channels between the ν^{th} left and μ^{th} right free-space modes [23]. It can be decomposed as $T_{\mu\nu} = \sum_{n=0}^{\infty} \sum_{s \in \mathcal{S}_n} A_{\mu\nu}^{s_n} e^{i\phi_{\mu\nu}^s}$, where \mathcal{S}_n denotes the set of all n -loop scattering paths, each specified by $s = (\alpha_1, \beta_1, \dots, \alpha_n, \beta_n, \alpha_{n+1})$. The amplitude along a single path is $A_{\mu\nu}^s = T_2 \mu \alpha_{n+1} \prod_{j=1}^n R_3 \alpha_{j+1} \beta_j R_2 \beta_j \alpha_j T_1 \alpha_1 \nu$, and the accumulated phase is $\phi_{\mu\nu}^s = \sum_{j=1}^{n+1} k_{\alpha_j} L - \sum_{j=1}^n k_{\beta_j} L$.

The transmission matrix oscillates with energy E and size L due to Fabry-Pérot interference [24]. In the thermodynamic limit $L \rightarrow \infty$, phase variation with E becomes arbitrarily rapid. Thus we can define the

smoothed transmittance between two Bloch modes

$$\bar{T}_{\mu\nu}(E) = \lim_{\delta E \rightarrow 0} \frac{1}{\delta E} \int_{E-\delta E/2}^{E+\delta E/2} |T_{\mu\nu}(\epsilon)|^2 \frac{Y_{\mu}^{\dagger} J Y_{\mu}}{Y_{\nu}^{\dagger} J Y_{\nu}} d\epsilon, \quad (12)$$

with the limit $L\delta E \rightarrow \infty$. In this limit, $\bar{T}_{\mu\nu}$ directly corresponds to the zero-temperature conductance between modes μ and ν for a long sample, up to the conventional quantum of conductance $G_{\mu\nu} = (2e^2/h)\bar{T}_{\mu\nu}$. Expanding $T_{\mu\nu}(E + \delta E)$ and keeping only propagating Bloch waves, one obtains $T_{\mu\nu}(E + \delta E) = \sum_{n=0}^{\infty} \sum_{s \in \mathcal{S}_n} A_{\mu\nu}^s \exp[i\phi_{\mu\nu}^s + i\delta E \tau_w^s]$, where the Wigner time delay is $\tau_w^s = L(\sum_{j=1}^{n+1} v_{g,\alpha_j}^{-1} - \sum_{j=1}^n v_{g,\beta_j}^{-1})$ and $v_{g,m} = \partial E / \partial k_m$ [25]. For large L , the smoothed transmittance can be expressed by Parseval's theorem as [26]:

$$\bar{T}_{\mu\nu}(E) = \frac{Y_{\mu}^{\dagger} J Y_{\mu}}{Y_{\nu}^{\dagger} J Y_{\nu}} \sum_{\tau} \left| \sum_{s \in \mathcal{S}_{\tau}} A_{\mu\nu}^s e^{i\phi_{\mu\nu}^s} \right|^2, \quad (13)$$

where \mathcal{S}_{τ} denotes the set of paths with Wigner time delay τ , showing that amplitudes with the same Wigner time delay add coherently, while contributions with different delays add incoherently [21].

Adiabatic Boundary and Topological Transmittance.— In Floquet lattices, temporal periodicity couples multiple sidebands, which generically complicates scattering at a boundary and obscures the direct correspondence between bulk band topology and transmission spectra [11–13]. This stands in contrast to static systems, where Bragg scattering provides a definitive rule: transmittance vanishes when the incident energy lies within a band gap, because scattering at a sharp boundary typically involves only a single Bloch mode. A key challenge is therefore to engineer a boundary condition for Floquet systems that suppresses multi-mode scattering, thereby enabling a clean extraction of bulk topological invariants, such as the winding number C , from transmission measurements [17, 27, 28].

To this end, we introduce an *adiabatic boundary* [29, 30]. The core idea is to avoid an abrupt interface by smoothly ramping up the Floquet potential. We parameterize the potential as $V_{\text{FL}}(x, t; \xi)$ and consider a spatial gradient in ξ from 0 (free space) to 1 (full Floquet lattice). By partitioning this gradient region into N_s segments with a small parameter increment $\delta\xi = 1/N_s$ per segment, scattering at each intermediate interface is dominated by a single transmitted mode. The transmittance between matched Bloch modes \bar{T}_{mm} scales as $1 + O(\delta\xi^2)$ where $\bar{T}_{\mu\nu} \equiv |T_{\mu\nu}|^2 (Y_{\mu}^{\dagger} J Y_{\mu}) / (Y_{\nu}^{\dagger} J Y_{\nu})$ [21]. In the adiabatic limit ($N_s, L_0 \rightarrow \infty$ where L_0 is the segment length), the total smoothed transmittance between connected modes \bar{T}_{mm} approaches unity, effectively suppressing all reflection and sideband transmission.

As a concrete example, we implement a staircase ramp $\xi(x) = \max(0, \min(1, \lfloor x/L \rfloor / N_s))$ for the potential $V(x, t) = \xi(x) [8 \cos(2\pi x - \omega t) + 2]$ (Fig. 3). This connects free space to a traveling-wave Floquet lattice whose

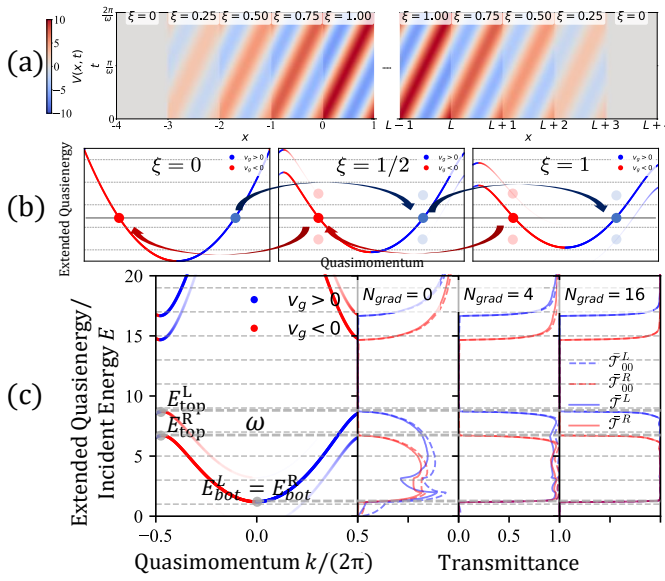


FIG. 3. (a) Potential profile with an adiabatic staircase gradient ($N_{\text{grad}} = N_s - 1 = 3$, $L_0 = 1$), defined by $V(x, t; \xi) = 8\xi \cos(2\pi x/d - \omega t) + 2\xi$. (b) Schematic of the one-to-one mapping between incident waves and Floquet-Bloch states enabled by the adiabatic boundary. (c) Quasi-energy band structure, total transmittance $\bar{T} = \sum_n \bar{T}_{n0}$, and same-mode transmittance \bar{T}_{00} for left/right incidence with varying N_{grad} . The homogeneous lattice region ($\xi = 1$) is sufficiently long $L \rightarrow \infty$.

quasi-energy band possesses a winding number $C = 1$ without spurious anticrossings [19].

This adiabatic boundary establishes a one-to-one mapping between each incident free-space plane wave and a corresponding propagating Floquet-Bloch state, provided they share the same quasi-energy and the same sign of the group velocity. As a result, a topologically non-trivial Floquet band ($C \neq 0$) enforces a rigid offset between the sets of quasi-energies that support perfect transmission for left- and right-moving incident waves. Accordingly, the transmission spectra consist of sharp energy windows represented by step function Θ , $\bar{T}^L(E) = \Theta(E - E_{\text{bot}}^L) - \Theta(E - E_{\text{top}}^L)$ and $\bar{T}^R(E) = \Theta(E - E_{\text{bot}}^R) - \Theta(E - E_{\text{top}}^R)$, whose widths satisfy $E_{\text{top}}^L - E_{\text{bot}}^L = E_{\text{top}}^R - E_{\text{bot}}^R + C\hbar\omega$ for an isolated Floquet band. Consequently, the integrated transmittance imbalance obeys

$$\int_{\min(E_{\text{bot}}^L, E_{\text{bot}}^R)}^{\max(E_{\text{top}}^L, E_{\text{top}}^R)} [\bar{T}^L(E) - \bar{T}^R(E)] dE = C\hbar\omega. \quad (14)$$

Therefore, the transmission windows for left and right incidence are shifted relative to each other by exactly $C\hbar\omega$, providing a direct and robust experimental signature of the bulk topological invariant C . Finally, using the Floquet transfer matrix framework, we get the topological transmittance under adiabatic boundary conditions, which is the most important result in our work.

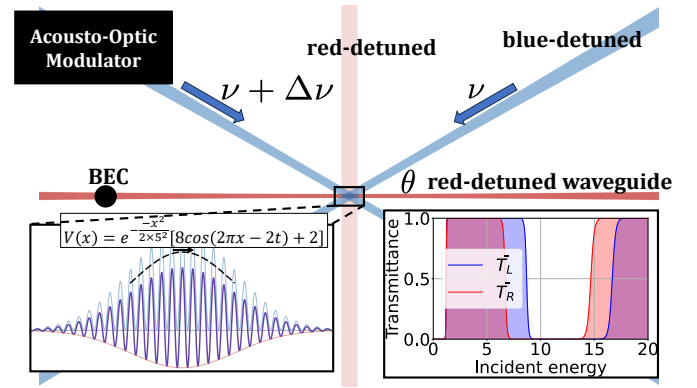


FIG. 4. Schematic of the cold-atom setup. Bottom right plots transmission spectrum for $V(x, t; \xi) = 8\xi \cos(2\pi x - 2t) + 2\xi$ with $\xi(x) = e^{-x^2/50}$.

Fig. 3 illustrates the potential profile, the mapping principle, and key numerical results. Simulations confirm that even a few gradient segments with $L_0 = 1$ are sufficient to achieve high-fidelity single-mode transmission.

Experimental considerations.— After introducing scattering state theory and topological transmittance, we now propose experimental platforms to test our theory.

Cold atoms. Cold-atom systems are ideal for quantum simulation due to their cleanliness and tunability [31]. They allow flexible construction of potentials, enabling direct tests of scattering in traveling-wave potentials with adiabatic boundaries [32]. As shown in Fig. 4, a red-detuned laser confines atoms in a 1D channel. Two blue-detuned lasers create a moving cosine potential via frequency modulation, while an additional red-detuned laser adjusts the barrier height for Bloch-wave matching. The Gaussian beam profiles naturally provide adiabatic boundaries. Bose-Einstein condensates (BEC) serve as 1D scatterers, similar to the setup of Fabre et al. [33].

Surface acoustic wave current. In electronic transport, the Landauer-Büttiker formula relates scattering to current [34–37]. Its Floquet extension is

$$I = \frac{2e}{h} \int_0^\infty dE \sum_{n=-\infty}^{\infty} [\bar{T}_{n0}^L(E) f_L(E) - (R \leftrightarrow L)], \quad (15)$$

where $f_{L/R}$ are the lead Fermi-Dirac distributions [10]. In static systems, reciprocity enforced by time-reversal symmetry ensures that the net transport current vanishes under zero-bias conditions [38]. Floquet driving breaks time-reversal symmetry, enabling a finite zero-bias current. Experimentally, a surface acoustic wave (SAW) on a piezoelectric substrate generates a traveling potential via an interdigital transducer driven at frequency f . Reflections are suppressed to create a traveling-wave potential with period $d = v/f$ (v is the sound velocity) in the scattering region.

We study the setup in Fig. 5(a): a SAW-induced potential in a quantum wire, with a trapezoidal top-gate.

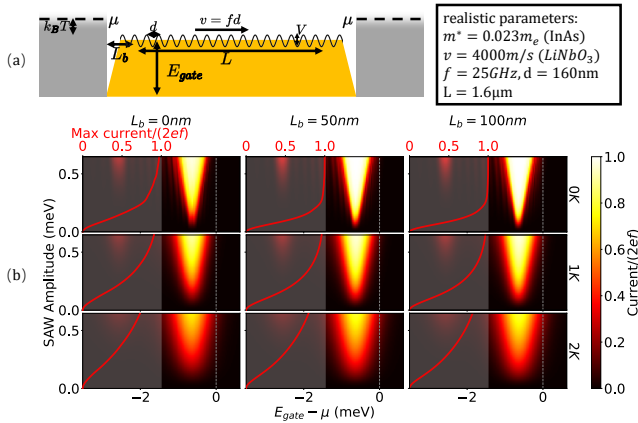


FIG. 5. (a) Modeling and parameter selection for the surface acoustic wave transport experiment. (b) With the above parameters, temperature and top-gate boundary length are scanned to calculate the bias-free transport current as functions of driving strength and gate voltage, where the chemical potential μ is set to 10 meV. The red line plots the maximum current for a given SAW amplitude during a gate voltage scan.

The zero-bias current is measured versus top-gate voltage (numerical results in Fig. 5(b)). At 1 K, a current near $2ef$ is detectable. For strong fields ($V \gg E_R = h^2/(8m^*d^2)$), localization leads to Coulomb blockade and a $1ef$ plateau [39–42]. Here we focus on $V < E_R$, where states are extended. Scattering-state theory gives a near $2ef$ quantized plateau with spin degeneracy.

Discussion and conclusion.— We have established a rigorous Floquet scattering theory for extended lattices using a conjugate symplectic transfer matrix framework. This symplectic structure ensures time-averaged probability current conservation and underpins the reciprocal eigenvalue pairing and balanced left/right propagating modes, which are essential for a well-posed multi-channel sideband scattering problem.

By introducing a spatial adiabatic boundary, we map the bulk topological winding number C directly to the transmission spectrum, predicting a rigid shift of $C\hbar$ in transmission windows—a signature testable in cold-atom Bragg scattering experiments. Applying the framework to SAW-driven quantum wires further reveals a robust zero-bias current plateau near $2ef$. This near-quantized transport, emerging even without adiabatic ramping, underscores the resilience of the underlying scattering physics. Our work provides both a versatile numerical tool and a clear conceptual link between Floquet-Bloch topology and observable transport phenomena.

Acknowledgments

We are grateful to Fangcheng Wang for pointing out that the constrained form of the transfer matrix corre-

sponds to a symplectic structure. We are also grateful to Carlo Beenakker for helpful discussions on MathOverflow regarding the structure of the symplectic group, and to Federico Poloni for pointing out relevant mathematical literature [22, 43]. X.D. Dai acknowledges the support from the New Cornerstone Foundation. X. Dai is supported by the New Cornerstone Foundation and a fellowship and a CRF award from the Research Grants Council of the Hong Kong Special Administrative Region, China (Projects No. HKUST SRFS2324-6S01 and No. C7037-22GF).

* daix@ust.hk

- [1] N. Ashcroft and N. Mermin, *Solid State Physics* (Holt, Rinehart and Winston, 1976).
- [2] F. Bloch, Über die quantenmechanik der elektronen in kristallgittern, *Zeitschrift für Physik* **52**, 555–600 (1929).
- [3] R. D. L. Kronig and W. G. Penney, Quantum mechanics of electrons in crystal lattices, *Proceedings of the Royal Society of London. Series A, Containing Papers of a Mathematical and Physical Character* **130**, 499–513 (1931).
- [4] A. H. Wilson, The theory of electronic semi-conductors, *Proceedings of the Royal Society of London. Series A, Containing Papers of a Mathematical and Physical Character* **133**, 458–491 (1931).
- [5] G. Floquet, Sur les équations différentielles linéaires à coefficients périodiques, *Annales scientifiques de l'École normale supérieure* **12**, 47–88 (1883).
- [6] J. H. Shirley, Solution of the schrödinger equation with a hamiltonian periodic in time, *Physical Review* **138**, B979–B987 (1965).
- [7] H. Sambe, Steady states and quasienergies of a quantum-mechanical system in an oscillating field, *Physical Review A* **7**, 2203–2213 (1973).
- [8] T. Oka and H. Aoki, Photovoltaic hall effect in graphene, *Phys. Rev. B* **79**, 081406 (2009).
- [9] N. H. Lindner, G. Refael, and V. Galitski, Floquet topological insulator in semiconductor quantum wells, *Nature Physics* **7**, 490–495 (2011).
- [10] M. Moskalets and M. Büttiker, Floquet scattering theory of quantum pumps, *Phys. Rev. B* **66**, 205320 (2002).
- [11] A. Emmanouilidou and L. E. Reichl, Floquet scattering and classical-quantum correspondence in strong time-periodic fields, *Phys. Rev. A* **65**, 033405 (2002).
- [12] W. Li and L. E. Reichl, Floquet scattering through a time-periodic potential, *Phys. Rev. B* **60**, 15732 (1999).
- [13] D. F. Martinez and L. E. Reichl, Transmission properties of the oscillating δ -function potential, *Phys. Rev. B* **64**, 245315 (2001).
- [14] F. Kang and Q. Mengzhao, *Symplectic Geometric Algorithms for Hamiltonian Systems* (2010).
- [15] H. Weyl, *The Classical Groups: Their Invariants and Representations* (Princeton University Press, Princeton, NJ, 1939).
- [16] J. Pendry, Symmetry and transport of waves in one-dimensional disordered systems, *Advances in Physics* **43**, 461–542 (1994).

- [17] T. Kitagawa, E. Berg, M. Rudner, and E. Demler, Topological characterization of periodically driven quantum systems, *Phys. Rev. B* **82**, 235114 (2010).
- [18] D. J. Thouless, Quantization of particle transport, *Phys. Rev. B* **27**, 6083 (1983).
- [19] L. Privitera, A. Russomanno, R. Citro, and G. E. Santoro, Nonadiabatic breaking of topological pumping, *Phys. Rev. Lett.* **120**, 106601 (2018).
- [20] A conjugate symplectic matrix F is defined by the condition $F^\dagger J F = J$, which differs from the standard symplectic definition that utilizes the transpose operation, $S^T JS = J$.
- [21] See the Supplemental Material.
- [22] V. Mehrmann, V. Noferini, F. Tisseur, and H. Xu, On the sign characteristics of hermitian matrix polynomials, *Linear Algebra and its Applications* **511**, 328 (2016).
- [23] C. J. Fujiwara, K. Singh, Z. A. Geiger, R. Senaratne, S. V. Rajagopal, M. Lipatov, and D. M. Weld, Transport in floquet-bloch bands, *Phys. Rev. Lett.* **122**, 010402 (2019).
- [24] M. Born, E. Wolf, A. B. Bhatia, P. C. Clemmow, D. Gabor, A. R. Stokes, A. M. Taylor, P. A. Wayman, and W. L. Wilcock, *Principles of Optics: Electromagnetic Theory of Propagation, Interference and Diffraction of Light* (Cambridge University Press, 1999).
- [25] C. Texier, Wigner time delay and related concepts: Application to transport in coherent conductors, *Physica E: Low-dimensional Systems and Nanostructures* **82**, 16 (2016), frontiers in quantum electronic transport - In memory of Markus Büttiker.
- [26] W. Rudin, *Principles of Mathematical Analysis*, International series in pure and applied mathematics (McGraw-Hill, 1976).
- [27] M. S. Rudner, N. H. Lindner, E. Berg, and M. Levin, Anomalous edge states and the bulk-edge correspondence for periodically driven two-dimensional systems, *Phys. Rev. X* **3**, 031005 (2013).
- [28] M. H. Kolodrubetz, F. Nathan, S. Gazit, T. Morimoto, and J. E. Moore, Topological floquet-thouless energy pump, *Phys. Rev. Lett.* **120**, 150601 (2018).
- [29] D. Marcuse, Mode conversion caused by surface imperfections of a dielectric slab waveguide, *Bell System Technical Journal* **48**, 3187–3215 (1969).
- [30] D. Marcuse, *Theory of Dielectric Optical Waveguides* (Elsevier, 1991).
- [31] I. Bloch, J. Dalibard, and W. Zwerger, Many-body physics with ultracold gases, *Rev. Mod. Phys.* **80**, 885 (2008).
- [32] D. Schrader, S. Kuhr, W. Alt, M. Müller, V. Gomer, and D. Meschede, An optical conveyor belt for single neutral atoms, *Applied Physics B* **73**, 819–824 (2001).
- [33] C. M. Fabre, P. Cheiney, G. L. Gattobigio, F. Vermersch, S. Faure, R. Mathevet, T. Lahaye, and D. Guéry-Odelin, Realization of a distributed bragg reflector for propagating guided matter waves, *Phys. Rev. Lett.* **107**, 230401 (2011).
- [34] S. Datta, *Electronic Transport in Mesoscopic Systems* (Cambridge University Press, 1995).
- [35] R. Landauer, Spatial variation of currents and fields due to localized scatterers in metallic conduction, *IBM J. Res. Dev.* **1**, 223 (1957).
- [36] R. Landauer, Electrical resistance of disordered one-dimensional lattices, *Philosophical Magazine* **21**, 863–867 (1970).
- [37] M. Büttiker, Four-terminal phase-coherent conductance, *Phys. Rev. Lett.* **57**, 1761 (1986).
- [38] P. W. Brouwer, Scattering approach to parametric pumping, *Phys. Rev. B* **58**, R10135 (1998).
- [39] N. E. Fletcher, J. Ebbecke, T. J. B. M. Janssen, F. J. Ahlers, M. Pepper, H. E. Beere, and D. A. Ritchie, Quantized acoustoelectric current transport through a static quantum dot using a surface acoustic wave, *Phys. Rev. B* **68**, 245310 (2003).
- [40] J. M. Shilton, D. R. Mace, V. I. Talyanskii, M. Y. Simmons, M. Pepper, A. C. Churchill, and D. A. Ritchie, Experimental study of the acoustoelectric effects in gaas-algaas heterostructures, *Journal of Physics: Condensed Matter* **7**, 7675–7685 (1995).
- [41] J. M. Shilton, D. R. Mace, V. I. Talyanskii, M. Pepper, M. Y. Simmons, A. C. Churchill, and D. A. Ritchie, Effect of spatial dispersion on acoustoelectric current in a high-mobility two-dimensional electron gas, *Phys. Rev. B* **51**, 14770 (1995).
- [42] J. M. Shilton, V. I. Talyanskii, M. Pepper, D. A. Ritchie, J. E. F. Frost, C. J. B. Ford, C. G. Smith, and G. A. C. Jones, High-frequency single-electron transport in a quasi-one-dimensional gaas channel induced by surface acoustic waves, *Journal of Physics: Condensed Matter* **8**, L531–L539 (1996).
- [43] R. Zhang, Symplectic inner products of eigenvectors of complex symplectic matrix, MathOverflow (2025).
- [44] H. E. Haber, What is the group of conjugate symplectic matrices (2017).
- [45] A. S. Glasser, *Gauge Structure in Algorithms for Plasma Physics* (Princeton University, 2022).
- [46] J. F. Cornwell, *Group theory in physics: An introduction* (Academic press, 1997).

Supplemental Materials

A. Conjugate Symplectic Group

For all the conjugate symplectic (CSp) matrix S in the set G which satisfies the condition

$$S^\dagger JS = J, \quad (16)$$

we can prove that the set G is a group. Here J is the same signature matrix in the normal symplectic matrix.

1. Identity It is straightforward to check that the Identity I satisfies the condition $I^\dagger J I = J$.
2. Closure For any two elements S_1 and S_2 in the set G , let $S = S_1 S_2$ here and we have

$$S^\dagger JS = (S_1 S_2)^\dagger J (S_1 S_2) = S_2^\dagger S_1^\dagger J S_1 S_2 = J. \quad (17)$$

3. Associativity For any three elements S_1 , S_2 and S_3 , with the matrix multiplication we have

$$S_1 S_2 S_3 = (S_1 S_2) S_3 = S_1 (S_2 S_3). \quad (18)$$

4. Inverse element For any element S in the set G , then the inverse element S^{-1} satisfies

$$S^\dagger JS = J \rightarrow J = (S^\dagger)^{-1} JS^{-1} \rightarrow (S^{-1})^\dagger JS^{-1} = J. \quad (19)$$

Furthermore, it can be proved that the CSp group G is a Lie group. It is similar to the symplectic group and change the condition 'Transpose' to 'Hermitian Conjugate'. Then, we follow the procedure in Ref. [44, 45] to prove G is a Lie group.

The metric matrix J in the CSp group can be diagonalized by a unitary matrix U

$$\frac{1}{\sqrt{2}} \begin{pmatrix} I_n & -iI_n \\ I_n & iI_n \end{pmatrix} \begin{pmatrix} 0 & I_n \\ -I_n & 0 \end{pmatrix} \frac{1}{\sqrt{2}} \begin{pmatrix} I_n & I_n \\ -iI_n & -iI_n \end{pmatrix} = i \begin{pmatrix} I_n & 0 \\ 0 & -I_n \end{pmatrix}. \quad (20)$$

Here we define

$$U = \frac{1}{\sqrt{2}} \begin{pmatrix} I_n & I_n \\ iI_n & -iI_n \end{pmatrix}. \quad (21)$$

Then we have $U^\dagger J U = iI_{n,n}$, where $I_{n,n} = \text{diag}(1, 1, \dots, 1, -1, -1, \dots, -1)$ and the numbers of diagonal elements that equal to $+1, -1$ are all n . By the unitary transformation, we map the CSp matrix to a new matrix $P = U^\dagger S U$. Then we have

$$S^\dagger JS = J \rightarrow UP^\dagger U^\dagger J UP U^\dagger = J \rightarrow UP^\dagger (iI_{n,n}) PU^\dagger = J \rightarrow P^\dagger I_{n,n} P = I_{n,n}. \quad (22)$$

Therefore, the matrix P mapped from S is a pseudo unitary matrix defined by the constraint $P^\dagger I_{n,n} P = I_{n,n}$. The corresponding pseudo unitary group $U(n, n)$ is a continuous Lie group [46]. $U(n, n)$ has two connected components and the identity component can be generated by the exponential map of its Lie algebra $\mathfrak{u}(n, n)$. Since the unitary mapping between the CSp group G and the pseudo unitary group $U(n, n)$ is bijective and smooth, thus the CSp group G is also a continuous Lie group (Lie group isomorphism). Furthermore, G also has two connected components. Here we define the generator of the identity component as K

$$S = e^{\alpha K}, \quad \alpha \in \mathbb{R}. \quad (23)$$

and K satisfies the constraint

$$K^\dagger J + JK = 0. \quad (24)$$

It is straightforward to check that

$$K^\dagger J = -JK \rightarrow e^{\alpha K^\dagger} = e^{-\alpha JK J^{-1}} \rightarrow e^{\alpha K^\dagger} = J e^{-\alpha K} J^{-1} \rightarrow (e^{\alpha K})^\dagger J e^{\alpha K} = J. \quad (25)$$

Here the parameter α is real. The generator K has the following form

$$K = \begin{pmatrix} A & B \\ C & -A^\dagger \end{pmatrix}, \quad (26)$$

here the n by n off-diagonal block matrices are both hermitian $B^\dagger = B, C^\dagger = C$. The diagonal block matrix A is an element in $\text{GL}(n, \mathbb{C})$. It is obvious that when parameter $\alpha \rightarrow 0$, $S = e^{\alpha K}$ goes to identity which is in the identity component of CSp group G .

B. Spectrum pairing, J -orthogonality, and the diagonalizable case

We continue to use the notation of the main text. Let

$$F \in \mathbb{C}^{2N \times 2N}, \quad F^\dagger JF = J, \quad J = \begin{pmatrix} 0 & I_N \\ -I_N & 0 \end{pmatrix}.$$

We first state two basic lemmas about the spectrum and the J -inner product, then give a constructive extension of Lemma 2 that covers the diagonalizable case with possible spectral degeneracies, and finally prove the existence of a generator G with

$$G^\dagger J + JG = 0, \quad e^G = F,$$

under the same diagonalizability assumption.

Lemma 1 (Spectrum reciprocal-conjugate pairing). *If $F^\dagger JF = J$ and $Fy = \lambda y$ with $y \neq 0$, then $1/\lambda^*$ is also an eigenvalue of F . A corresponding eigenvector may be taken proportional to Jz where $F^\dagger z = \lambda^* z$.*

Proof. From $F^\dagger JF = J$ we have $F = -JF^{-\dagger}J$. Apply both sides to Jz to obtain

$$F(Jz) = \frac{1}{\lambda^*} (Jz),$$

so $1/\lambda^* \in \sigma(F)$. \square

Lemma 2 (J -inner product orthogonality). *Let Y_m and Y_n be eigenvectors of F with eigenvalues λ_m and λ_n , respectively. If $\lambda_m^* \lambda_n \neq 1$, then*

$$Y_m^\dagger J Y_n = 0.$$

Proof. Using $F^\dagger JF = J$ and $FY_n = \lambda_n Y_n$, $FY_m = \lambda_m Y_m$, compute

$$Y_m^\dagger J Y_n = Y_m^\dagger F^\dagger J F Y_n = \lambda_m^* \lambda_n Y_m^\dagger J Y_n.$$

If $\lambda_m^* \lambda_n \neq 1$ the identity forces $Y_m^\dagger J Y_n = 0$. \square

We now state the constructive extension that handles spectral degeneracy under the assumption that F is diagonalizable (no nontrivial Jordan blocks).

Proposition 1 (Extended Lemma 2 — blockwise biorthogonalization in the diagonalizable case). *Suppose F satisfies $F^\dagger JF = J$ and is diagonalizable:*

$$F = SD_F S^{-1}, \quad S = [Y_1, \dots, Y_{2N}], \quad D_F = \text{diag}(\lambda_1, \dots, \lambda_{2N}).$$

Define the matrix of J -pairings

$$N \equiv S^\dagger JS, \quad N_{mn} = Y_m^\dagger J Y_n.$$

Partition the index set into equivalence classes generated by

$$m \sim n \iff \lambda_m^* \lambda_n = 1,$$

i.e. group together indices whose eigenvalues are reciprocal-conjugates. Then, by performing local linear transformations inside each such equivalence class, one can construct a new eigen-basis $\{\tilde{Y}_\alpha\}$ and corresponding dual row-vectors $\{\tilde{Y}_\alpha^\dagger\}$ that satisfy the global biorthonormality and completeness relations

$$\tilde{Y}_\alpha^\dagger \tilde{Y}_\beta = \delta_{\alpha\beta}, \quad \sum_{\alpha=1}^{2N} \tilde{Y}_\alpha \tilde{Y}_\alpha^\dagger = I_{2N}. \quad (27)$$

In other words, under the diagonalizability assumption the J -biorthogonal and completeness relations used in the main text can always be realized even in the presence of spectral degeneracies (subject to the caveat below concerning singular pairing blocks).

Proof. By Lemma 2, $N_{mn} = 0$ whenever $\lambda_m^* \lambda_n \neq 1$. Hence N is block-sparse with respect to the partition into equivalence classes: only entries within the same class may be nonzero. We therefore treat each class separately and then assemble the local constructions.

Paired class (two distinct reciprocal-conjugate eigenvalues). Consider an equivalence class consisting of two reciprocal-conjugate eigenvalues λ and $\bar{\lambda} := 1/\lambda^*$ with geometric multiplicity r each. Order the corresponding eigenvectors as

$$S_{\text{block}} = [U \mid V], \quad U = [u_1, \dots, u_r], \quad V = [v_1, \dots, v_r],$$

where the u 's correspond to λ and the v 's to $\bar{\lambda}$. Then the local pairing matrix has the structure

$$N_{\text{block}} = S_{\text{block}}^\dagger J S_{\text{block}} = \begin{pmatrix} 0 & M \\ -M^\dagger & 0 \end{pmatrix}, \quad M_{pq} = v_p^\dagger J u_q.$$

Assume M is invertible (the singular case is discussed below). Define the swap matrix

$$P = \begin{pmatrix} 0 & I_r \\ I_r & 0 \end{pmatrix},$$

and form

$$\mathcal{N} \equiv PN_{\text{block}} = \begin{pmatrix} -M^\dagger & 0 \\ 0 & M \end{pmatrix},$$

which is block-diagonal and invertible. Now set

$$S_{\text{block}}^\ddagger \equiv \mathcal{N}^{-1} P S_{\text{block}}^\dagger J.$$

A direct calculation yields

$$S_{\text{block}}^\ddagger S_{\text{block}} = \mathcal{N}^{-1} P S_{\text{block}}^\dagger J S_{\text{block}} = \mathcal{N}^{-1} P N_{\text{block}} = I_{2r}.$$

Hence the columns of S_{block} and the rows of $S_{\text{block}}^\ddagger$ form a local biorthonormal pair. Repeating this construction for every paired class and assembling the block-row matrices $S_{\text{block}}^\ddagger$ (in the same column order) produces a global row-matrix S^\ddagger satisfying $S^\ddagger S = I_{2N}$.

Self-paired class (eigenvalues on the unit circle). If an equivalence class consists of eigenvalues λ with $|\lambda| = 1$ (so $\bar{\lambda} = \lambda$), let W be the matrix of the corresponding eigenvectors (columns). Then the local pairing matrix is

$$N_{\text{block}} = W^\dagger J W,$$

which is skew-Hermitian. If N_{block} is invertible, set $\mathcal{N} = N_{\text{block}}$ and define

$$W^\ddagger \equiv \mathcal{N}^{-1} W^\dagger J,$$

to obtain $W^\ddagger W = I$. As before, concatenating these local duals gives a global S^\ddagger with $S^\ddagger S = I$.

Assembly and completeness. Assembling all local dual blocks into a single S^\ddagger yields $S^\ddagger S = I_{2N}$. Since S is invertible, we also have $SS^\ddagger = I_{2N}$, and therefore the identities (27) hold for the normalized column vectors \tilde{Y}_α and the corresponding row vectors $\tilde{Y}_\alpha^\ddagger$.

Singular pairing blocks (exceptional cases). The above local inversions require that the local pairing matrices (e.g. M or N_{block}) are invertible. If a block is singular, this indicates the existence of a J -neutral direction or a degenerate J -pairing inside that equivalence class. Such singularity is an additional algebraic constraint on the parameters (hence nongeneric). A practical remedy is:

Adding a small generic perturbation to F (or to the underlying potential) that breaks the special degeneracy, perform the blockwise construction on the perturbed matrix, and then take the perturbation to zero if the limit exists. \square

We now prove existence of a generator G in the Lie algebra defined by the infinitesimal CSp condition.

Theorem 1 (Exponential generation in the diagonalizable case). *Let F satisfy $F^\dagger J F = J$ and suppose F is diagonalizable: $F = S D_F S^{-1}$. Choose a branch of the complex logarithm for each eigenvalue and define*

$$D_G = \text{diag}(g_1, \dots, g_{2N}), \quad e^{D_G} = D_F,$$

with the branch choice made so that paired entries satisfy

$$g_{p(j)} = -g_j^*, \quad (28)$$

where $p(j)$ denotes the partner index of j (i.e., $\lambda_{p(j)} = 1/\lambda_j^*$). Define

$$G \equiv SD_G S^{-1}.$$

Then $e^G = F$ and $G^\dagger J + JG = 0$.

Proof. By definition of D_G we have $e^{D_G} = D_F$. Since S is invertible,

$$e^G = e^{SD_G S^{-1}} = S e^{D_G} S^{-1} = S D_F S^{-1} = F.$$

To verify the Lie-algebra condition $G^\dagger J + JG = 0$, we first note that from $F^\dagger JF = J$ and $F = SD_F S^{-1}$ we obtain

$$(S^{-1})^\dagger D_F^\dagger (S^\dagger JS) D_F S^{-1} = J.$$

Define the matrix $K \equiv S^\dagger JS$. The equation simplifies to

$$D_F^\dagger K D_F = K.$$

Since D_F is diagonal, this implies for each entry K_{ij} :

$$\lambda_i^* \lambda_j K_{ij} = K_{ij}.$$

Consequently, if $\lambda_i^* \lambda_j \neq 1$, then $K_{ij} = 0$. In particular, K_{ij} can be non-zero only when $\lambda_i^* \lambda_j = 1$.

Now compute $G^\dagger J + JG$. Using $G = SD_G S^{-1}$, we have

$$\begin{aligned} G^\dagger J + JG &= (S^{-1})^\dagger D_G^\dagger S^\dagger J + J S D_G S^{-1} \\ &= (S^{-1})^\dagger D_G^\dagger K S^{-1} + (S^\dagger)^{-1} K D_G S^{-1}. \end{aligned}$$

The second equality follows from $S^\dagger J = KS^{-1}$ and its conjugate transpose $JS = (S^\dagger)^{-1}K$.

Factor out the common terms:

$$G^\dagger J + JG = (S^{-1})^\dagger (D_G^\dagger K + K D_G) S^{-1}.$$

Because D_G is diagonal, the (i, j) -entry of the matrix in parentheses equals

$$(D_G^\dagger K + K D_G)_{ij} = g_i^* K_{ij} + K_{ij} g_j = (g_i^* + g_j) K_{ij}.$$

If $K_{ij} = 0$, the contribution vanishes trivially. If $K_{ij} \neq 0$, then by the observation above we must have $\lambda_i^* \lambda_j = 1$. The logarithm pairing condition (28) gives $g_j = -g_i^*$ (since $j = p(i)$), hence $g_i^* + g_j = 0$. Therefore every entry of $D_G^\dagger K + K D_G$ is zero, i.e.

$$D_G^\dagger K + K D_G = 0.$$

Finally,

$$G^\dagger J + JG = (S^{-1})^\dagger \cdot 0 \cdot S^{-1} = 0,$$

which completes the proof. □

C. Perturbation theory (diagonalizable hypothesis)

Setting. Let $Q(u)$ be a smooth one-parameter family of finite-dimensional CSp operators (or generators) depending on a real parameter u , and suppose $Q(0) = Q$ is diagonalizable. We consider a small perturbation

$$Q(u) = Q + uW + o(u),$$

with W a fixed matrix (not necessarily CSp). Denote an eigenpair of Q by

$$QY = \lambda Y,$$

where $Y \neq 0$. Let Y^\ddagger denote a left eigenvector (row vector) satisfying $Y^\ddagger Q = \lambda Y^\ddagger$ and normalized so that $Y^\ddagger Y = 1$ (such a biorthonormal pair exists for diagonalizable Q after appropriate local normalization; see main supplement).

(i) *Simple eigenvalue (non-degenerate).* Consider the perturbed eigenpair $(\lambda(u), Y(u))$ with $\lambda(0) = \lambda$, $Y(0) = Y$. Expand

$$(Q + uW)(Y + u\dot{Y}) + o(u) = (\lambda + u\dot{\lambda})(Y + u\dot{Y}) + o(u),$$

where $\dot{\lambda} = \frac{d\lambda}{du}\Big|_{u=0}$, $\dot{Y} = \frac{dY}{du}\Big|_{u=0}$. Collect $O(u)$ terms:

$$WY + (Q - \lambda)\dot{Y} = \dot{\lambda}Y. \quad (29)$$

Left-multiply by the dual row Y^\dagger . Using $Y^\dagger(Q - \lambda) = 0$ we obtain

$$\dot{\lambda} = Y^\dagger WY. \quad (30)$$

This is the standard first-order perturbation formula for a simple eigenvalue.

(ii) *Geometrically degenerate eigenvalue (multiplicity $m > 1$).* Assume λ has geometric multiplicity m . Choose a biorthonormal basis $\{Y_1, \dots, Y_m\}$ of the λ -eigenspace and corresponding left vectors $\{Y_1^\dagger, \dots, Y_m^\dagger\}$ such that $Y_i^\dagger Y_j = \delta_{ij}$ (possible under diagonalizability; see main supplement for constructive procedure). Expand a perturbed eigenvector inside this subspace:

$$Y(u) = \sum_{j=1}^m c_j(u) Y_j + Z(u), \quad Z(u) \perp\!\!\!\perp \text{(eigenspace)}.$$

Insert into $(Q + uW)Y(u) = \lambda(u)Y(u)$ and collect $O(u)$ terms, then project onto the i -th dual row Y_i^\dagger . Using $Y_i^\dagger(Q - \lambda) = 0$ and $Y_i^\dagger Z(0) = 0$, we obtain the $m \times m$ secular (matrix) equation:

$$\sum_{j=1}^m (Y_i^\dagger WY_j) c_j(0) = \dot{\lambda} c_i(0), \quad i = 1, \dots, m. \quad (31)$$

In matrix form $M\mathbf{c} = \dot{\lambda}\mathbf{c}$ with $M_{ij} = Y_i^\dagger WY_j$. Thus the admissible first-order splitting rates $\dot{\lambda}$ are the eigenvalues of the finite matrix M ; diagonalizing M yields the linear splitting directions and rates. In particular degeneracy is generically broken linearly.

D: Sign Equal Division Theorem

This part is to prove the current-balance property of the conjugate symplectic Floquet transfer matrix. The numbers of Bloch-wave eigenvalues with positive and negative time-averaged current are equal, $N_+ = N = N_B$. $\{Y_i\}$ are eigenvectors of Generator $G = \begin{pmatrix} A & B \\ C & -A^\dagger \end{pmatrix}$, where A is a $N \times N$ complex matrix, B and C are $N \times N$ Hermitian matrix. The number of $-iY^\dagger JY > 0$ is equal to $-iY^\dagger JY < 0$

Proof: Consider a polynomial:

$$\begin{aligned} p(i\lambda, u) &= \det(G - \lambda - uJ) \\ &= \det \begin{pmatrix} A - \lambda I & B - uI \\ C + uI & -A^\dagger - \lambda I \end{pmatrix} \end{aligned} \quad (32)$$

where u is real and λ is imaginary. what we concern is the solution of imaginary λ satisfied $p(i\lambda, 0) = 0$. These are eigenvalues corresponds to eigenvectors with $iY^\dagger JY \neq 0$

Now consider the perturbation forum.

$$(Y^\dagger JY) \frac{d(i\lambda)}{du}\Big|_{u=0} = iY^\dagger JWY \quad (33)$$

and set $W = -J$, then

$$\frac{du}{d(i\lambda)}\Big|_{u=0} = \frac{Y^\dagger JY}{iY^\dagger Y} \in [-1, 1] \quad (34)$$

This equation tells us that the $\text{sgn}(-iY^\dagger JY) = \text{sgn}(\frac{du}{d(i\lambda)}|_{u=0})$ which is the slope of the curve of $p(i\lambda, u) = 0$ at $u = 0$

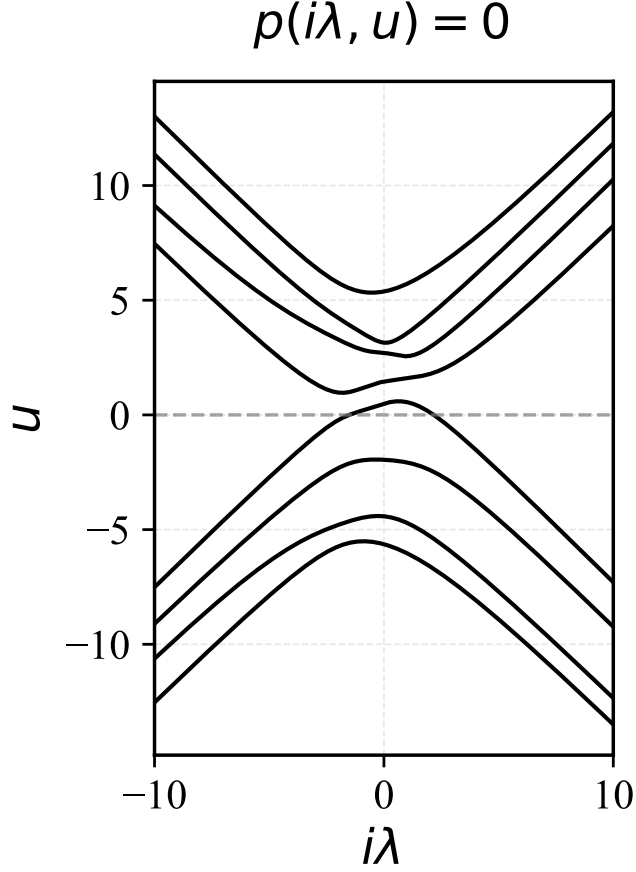


FIG. 6. Diagram of $p(i\lambda, u) = 0$.

Now consider $i\lambda \rightarrow \infty$. To make the polynomial equals to zero, there must be $\frac{|u|}{|\lambda|} \rightarrow 1$. So the curves can only have four types:

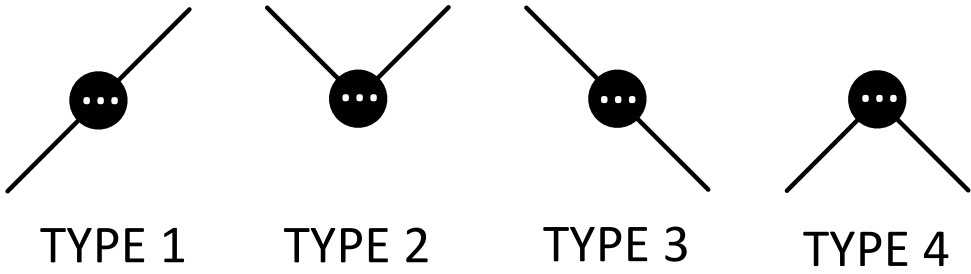


FIG. 7. Four types of curves in $(i\lambda, u)$ coordinate.

Consider the number of roots with $\frac{du}{d(i\lambda)} > 0$ as N_+ , $\frac{du}{d(i\lambda)} < 0$ as N_- . It is easy to find:

$$N = N_+ - N_- = N_1 + 0N_2 - N_3 + 0N_4 \quad (35)$$

where $N_{1,2,3,4}$ denotes number of each type of curves.

To prove the theorem, we only need to prove $N_1 = N_3$. Let's Consider another form of the polynomial.

$$\begin{aligned} p(i\lambda, u) &= \det \begin{pmatrix} B - uI & -A + \lambda I \\ -A^\dagger - \lambda I & -C - uI \end{pmatrix} \\ &= \det[H(\lambda) - uI] \end{aligned} \quad (36)$$

This is a characteristic polynomial of a Hermitian matrix. We can find that

$$\text{Tr}(H(\lambda)) = \sum u_i(\lambda) \quad (37)$$

is a invariant of λ . So there must be

$$\lim_{i\lambda \rightarrow +\infty} \frac{\sum u_i}{|i\lambda|} = \lim_{i\lambda \rightarrow -\infty} \frac{\sum u_i}{|i\lambda|} = 0 \quad (38)$$

We can also find

$$\lim_{i\lambda \rightarrow +\infty} \frac{\sum u_i}{|i\lambda|} - \lim_{i\lambda \rightarrow -\infty} \frac{\sum u_i}{|i\lambda|} = 2(N_1 - N_3) \quad (39)$$

Thus $N_1 - N_3 = 0$. Q.E.D.

E. Symplectic integrator

In practical calculations of the Floquet transfer matrix, preservation of the conjugate symplectic (CSp) structure requires two conditions:

1. the generator $G(x)$ satisfies the infinitesimal CSp condition $G^\dagger J + JG = 0$;
2. the numerical scheme used to integrate the generator is symplectic, so that the resulting transfer matrix satisfies $F^\dagger JF = J$.

Condition 1: CSp property of the generator. In our problem the wave-function vector satisfies

$$\frac{d}{dx} Y(x) = G(x)Y(x), \quad G(x) = \begin{pmatrix} 0 & I \\ M(x) & 0 \end{pmatrix}. \quad (40)$$

Substituting this form into the infinitesimal CSp condition shows that it reduces to the Hermiticity of the matrix $M(x)$,

$$M(x) = M^\dagger(x).$$

Using

$$M_{mn} = -(\epsilon + n\omega)\delta_{mn} + V_{m-n}(x),$$

this condition is guaranteed by the reality of the time-dependent potential $V(x, t)$. In numerical calculations it is therefore sufficient to adopt a frequency cutoff that does not break the Hermiticity of M . A simple symmetric truncation of Fourier modes already satisfies this requirement.

Condition 2: Symplectic integration scheme. The essential requirement of a symplectic integrator is that the local propagation operator

$$F(x_0 + \frac{\Delta x}{2}, x_0 - \frac{\Delta x}{2}) = \exp(G(x_0)\Delta x)$$

satisfies the CSp condition $F^\dagger JF = J$. An exact evaluation of the matrix exponential always preserves this structure, and this approach is adopted in our numerical implementation.

If one wishes to reduce computational complexity, a structure-preserving stepwise update can also be employed. For example, a simple symplectic approximation of the local transfer matrix reads

$$F(x_0 + \frac{\Delta x}{2}, x_0 - \frac{\Delta x}{2}) = I + \begin{pmatrix} 0 & I\Delta x + M^2(\Delta x)^2 \\ M\Delta x & 0 \end{pmatrix}, \quad (41)$$

which maintains the conjugate symplectic structure to the given order.

F. Smoothed transmittance

We complement the discussion in the main text by giving a self-contained derivation and practical recipe for the smoothed transmission matrix in the thermodynamic limit. Starting from the path expansion (main text),

$$T_{\mu\nu}(E) = \sum_{n=0}^{\infty} \sum_{s \in \mathcal{S}_n} A_{\mu\nu}^s e^{i\phi_{\mu\nu}^s(E)}, \quad (42)$$

each scattering path is denoted

$$s = (\alpha_1, \beta_1, \dots, \alpha_n, \beta_n, \alpha_{n+1}),$$

where the α_j (β_j) index forward (backward) propagating Bloch channels inside the central Floquet region. The amplitude of a single path is

$$A_{\mu\nu}^s = T_{2,\mu\alpha_{n+1}} \prod_{j=1}^n (R_{3,\alpha_{j+1}\beta_j} R_{2,\beta_j\alpha_j}) T_{1,\alpha_1\nu},$$

and the accumulated phase is

$$\phi_{\mu\nu}^s(E) = \sum_{j=1}^{n+1} k_{\alpha_j}(E) L - \sum_{j=1}^n k_{\beta_j}(E) L,$$

with L the length (number of unit cells) of the central region.

Wigner time delay and path counting vector The Wigner time delay associated to path s is

$$\tau_w^s = L \left(\sum_{j=1}^{n+1} v_{g,\alpha_j}^{-1} - \sum_{j=1}^n v_{g,\beta_j}^{-1} \right), \quad v_{g,m} = \frac{\partial E}{\partial k_m}. \quad (43)$$

To group paths that share the same delay we introduce a path-count vector

$$\mathbf{N} \equiv (N_1^+, N_2^+, \dots; N_1^-, N_2^-, \dots),$$

where N_m^+ (N_m^-) is the number of times the m -th Bloch channel appears as a forward (backward) segment in the path. Under generic conditions (absence of time-reversal symmetry constraints or exact degeneracies) paths with the same τ_w correspond to the same counting vector \mathbf{N} ; i.e. $\tau_w = \tau(\mathbf{N})$ and we partition the entire path set as

$$\mathcal{S} = \bigcup_{\mathbf{N}} \mathcal{S}_{\mathbf{N}}, \quad \tau_w^s = \tau(\mathbf{N}) \text{ for } s \in \mathcal{S}_{\mathbf{N}}.$$

Parseval regrouping Using this partition, the smoothed transmittance given by Parseval's theorem in the main text,

$$\bar{T}_{\mu\nu}(E) = \frac{Y_{\mu}^{\dagger} J Y_{\mu}}{Y_{\nu}^{\dagger} J Y_{\nu}} \sum_{\tau} \left| \sum_{s \in \mathcal{S}_{\tau}} A_{\mu\nu}^s e^{i\phi_{\mu\nu}^s(E)} \right|^2,$$

can be rewritten equivalently as a sum over counting vectors,

$$\bar{T}_{\mu\nu}(E) = \frac{Y_{\mu}^{\dagger} J Y_{\mu}}{Y_{\nu}^{\dagger} J Y_{\nu}} \sum_{\mathbf{N}} \left| \sum_{s \in \mathcal{S}_{\mathbf{N}}} A_{\mu\nu}^s e^{i\phi_{\mu\nu}^s(E)} \right|^2. \quad (44)$$

Equation (44) makes explicit that amplitudes from paths with the same counting vector (hence same Wigner delay) coherently add, while contributions from distinct \mathbf{N} add incoherently after the smoothing.

From a computational viewpoint one may enumerate contributions by increasing $\sum_m (N_m^+ + N_m^-)$ and truncate when the accumulated amplitudes become negligible; each extra round-trip introduces additional reflection factors so that amplitudes typically decay rapidly with total traversal number, ensuring good convergence.

Phase representation and ergodic averaging Equivalently, the transmission depends on the propagation phases of the propagating Bloch modes. Let N_B be the number of propagating (Bloch) channels at the energy of interest in a direction, and define

$$\theta_j(E) \equiv k_j(E) L \pmod{2\pi}, \quad j = 1, \dots, 2N_B.$$

Then the transmission matrix element is a periodic function of these phases,

$$T_{\mu\nu}(E) =: f_{\mu\nu}(\theta_1(E), \dots, \theta_{2N_B}(E)).$$

If the set of inverse group velocities $\{v_{g,j}^{-1}\}$ is in generic position (in particular if the ratios $v_{g,i}^{-1}/v_{g,j}^{-1}$ are rationally independent), then as $L \rightarrow \infty$ the phase vector $(\theta_1(E), \dots, \theta_{2N_B}(E))$ equidistributes on the torus \mathbb{T}^{2N_B} when E is varied. Under this ergodicity/equidistribution assumption the energy smoothing is equivalent to a uniform phase average:

$$\bar{T}_{\mu\nu}(E) = \frac{Y_\mu^\dagger J Y_\mu}{Y_\nu^\dagger J Y_\nu} \frac{1}{(2\pi)^{2N_B}} \int_{[0,2\pi]^{2N_B}} |f_{\mu\nu}(\theta_1, \dots, \theta_{2N_B})|^2 d^{2N_B} \theta. \quad (45)$$

Expanding $f_{\mu\nu}$ in the Fourier basis of the torus, orthogonality of the exponentials implies that cross terms between distinct multi-index Fourier components vanish under the phase integral; grouping Fourier components by the same multi-index is precisely equivalent to grouping scattering paths by the same counting vector \mathbf{N} . Hence (45) is algebraically equivalent to (44).

Numerical implementation (Monte Carlo over phases) Equation (45) furnishes a straightforward numerical protocol:

1. Replace each propagating factor $e^{ik_j L}$ by an independent phase variable $e^{i\theta_j}$, forming $T_{\mu\nu}(\{\theta_j\})$.
2. Draw S independent samples $\{\theta^{(s)}\}_{s=1}^S$ uniformly from $[0, 2\pi)^{2N_B}$.
3. Estimate the smoothed element by the sample mean

$$\hat{\bar{T}}_{\mu\nu} = \frac{Y_\mu^\dagger J Y_\mu}{Y_\nu^\dagger J Y_\nu} \frac{1}{S} \sum_{s=1}^S |T_{\mu\nu}(\{\theta^{(s)}\})|^2.$$

G: Floquet Adiabatic Boundary

Consider two Floquet lattices parameterized by $\xi = 0$ and $\xi = 1$, respectively. We construct a continuous path in the parameter space where ξ varies from 0 to 1, with each ξ corresponding to a Floquet lattice whose potential varies continuously with ξ . Since the quasi-energy $E_{v_g=0,m}$ at the band bottom or top serves as a characteristic feature and differs between $\xi = 0$ and $\xi = 1$, we assume (or require) that along this path, $\delta E_{v_g=0,m} = O(\delta\xi)$.

We aim to prove that if a Bloch wave mode at $\xi = 0$ connects adiabatically to a Bloch wave mode at $\xi = 1$ without undergoing any band transition (i.e., without merging with another Bloch wave and converting into two evanescent waves), then the current transmittance between Bloch waves for two Floquet lattices separated by $O(\delta\xi)$ along the path satisfies $1 - O((\delta\xi)^2)$.

Away from band top/bottom

We first consider the simplest case where the transfer matrix spectrum at a given quasi-energy undergoes no Bloch-to-evanescent pair-merging transition along the parameter path. In this case, all Wave Function Vectors (WFVs) can be current-normalized without divergence:

$$\bar{Y}^\dagger J Y = \pm i. \quad (46)$$

For Bloch waves, their WFVs are self-dual. Thus, the constraint on $Y = [\Phi, \Phi']^T$ can be written as:

$$\delta\Phi^\dagger\Phi' + \Phi^\dagger\delta\Phi' - \delta\Phi'^\dagger\Phi - \Phi'^\dagger\delta\Phi = 0. \quad (47)$$

From this, we derive:

$$\text{Im}(\delta\Phi^\dagger\Phi' - \delta\Phi'^\dagger\Phi) = 0. \quad (48)$$

The transfer matrix is given by:

$$T_L = \left(A_\oplus^\dagger(\xi) A_\oplus(\xi + \delta\xi) \right)^{-1}, \quad (49)$$

and its inverse is:

$$T_L^{-1} = A_\oplus^\dagger(\xi) A_\oplus(\xi + \delta\xi). \quad (50)$$

For the WVF of Bloch waves:

$$\begin{pmatrix} \Phi + \delta\Phi \\ \Phi' + \delta\Phi' \end{pmatrix}^\dagger J \begin{pmatrix} \Phi \\ \Phi' \end{pmatrix} = \pm i + (\delta\Phi^\dagger\Phi' - \delta\Phi'^\dagger\Phi) \quad (51)$$

$$= \pm i + O(\Re[\delta\xi]). \quad (52)$$

For Bloch wave modes m_B , we have:

$$T_{L,m_B m_B}^{-1} = 1 + \text{Im}(O(\delta\xi)) + O(\delta\xi^2). \quad (53)$$

For evanescent wave modes m_E :

$$T_{L,m_E m_E}^{-1} = 1 + O(\delta\xi). \quad (54)$$

The off-diagonal elements are all of order $O(\delta\xi)$.

Since the matrix approaches the identity matrix in the limit $\delta\xi \rightarrow 0$, its inverse can be expressed using the Neumann series. It follows that for Bloch waves, the diagonal transmittance coefficient is $1 + \text{Im} O(\delta\xi) + O(\delta\xi^2)$, and thus $|T_{m_B m_B}| = 1 + O(\delta\xi^2)$.

Near band top/bottom

Now consider the more general case where the path crosses a band bottom or top. Except for the measure-zero case of landing exactly on the band edge, two closely spaced points on the path may approach a transition point, causing the symplectic inner product to vanish and the normalization coefficient to diverge.

Consider two pathological points located at distances $O(\Delta_1)$ and $O(\Delta_2)$ from the transition point, with $\Delta_{1,2} < \delta\xi$ and at least one $\Delta = O(\delta\xi)$. We can express:

$$T^{-1} = D_1 \left[\begin{array}{ccc|cc|cc} 1 + \Im O(\delta\xi) & O(\delta\xi) & \cdots & O(\delta\xi) & \cdots & O(\delta\xi) \\ O(\delta\xi) & 1 + \Im O(\delta\xi) & \cdots & O(\delta\xi) & \cdots & O(\delta\xi) \\ \vdots & \vdots & \ddots & \vdots & \ddots & \vdots \\ \hline O(\delta\xi) & O(\delta\xi) & \cdots & O(\Delta_1^{1/2}) + O(\Delta_2^{1/2}) & \cdots & O(\delta\xi) \\ \hline \vdots & \vdots & \ddots & \vdots & \ddots & \vdots \\ O(\delta\xi) & O(\delta\xi) & \cdots & O(\delta\xi) & \cdots & 1 + O(\delta\xi) \end{array} \right] D_2 \quad (55)$$

where the scaling matrices are:

$$D_1 = \text{diag}(1, \dots, 1, O(\Delta_1^{-1/4}), 1, \dots, 1), \quad (56)$$

$$D_2 = \text{diag}(1, \dots, 1, O(\Delta_2^{-1/4}), 1, \dots, 1). \quad (57)$$

The labeled rows and columns correspond to WFVs crossing band edges. Since their current tends to zero, the current normalization coefficient diverges. We normalize only their wavefunction part and incorporate the divergent normalization coefficients into the scaling matrices D_1 and D_2 . Given the quadratic dispersion relation at band edges,

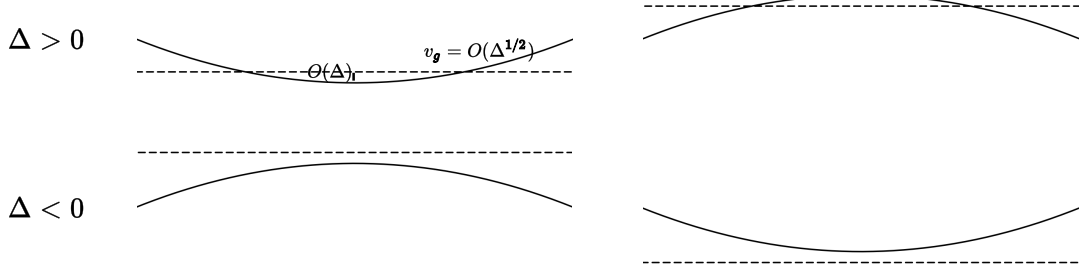


FIG. 8. Situation near band top/bottom

the current of wavefunction-normalized states scales as $\sqrt{\Delta}$, with normalization coefficients scaling as $\Delta^{-1/4}$. The variation of WFs is also consistent with current scaling as $\sqrt{\Delta}$.

For any combination of signs of Δ_1 and Δ_2 , the absolute value of the center element is either $|O(\Delta_1)|^{1/2} + |O(\Delta_2)|^{1/2}$ or $\sqrt{|O(\Delta_1)| + |O(\Delta_2)|}$, both of which are $O(\delta\xi^{1/2})$.

Thus, we have:

$$T = D_2^{-1} \begin{bmatrix} 1 + \Im O(\delta\xi) & O(\delta\xi) & \cdots & | & O(\delta\xi) & \cdots & O(\delta\xi) \\ O(\delta\xi) & 1 + \Im O(\delta\xi) & \cdots & | & O(\delta\xi) & \cdots & O(\delta\xi) \\ \vdots & \vdots & \ddots & | & \vdots & \ddots & \vdots \\ \hline O(\delta\xi) & O(\delta\xi) & \cdots & | & O(\delta\xi^{1/2}) & \cdots & O(\delta\xi) \\ \vdots & \vdots & \ddots & | & \vdots & \ddots & \vdots \\ \hline O(\delta\xi) & O(\delta\xi) & \cdots & | & O(\delta\xi) & \cdots & 1 + O(\delta\xi) \end{bmatrix}^{-1} D_1^{-1} \quad (58)$$

Introducing an additional scaling matrix $D_0 = \text{diag}(1, \dots, 1, O(\delta\xi^{-1/4}), 1, \dots, 1)$, we obtain:

$$T = D_2^{-1} D_0 \begin{bmatrix} 1 + \Im O(\delta\xi) & O(\delta\xi) & \cdots & | & O(\delta\xi^{5/4}) & \cdots & O(\delta\xi) \\ O(\delta\xi) & 1 + \Im O(\delta\xi) & \cdots & | & O(\delta\xi^{5/4}) & \cdots & O(\delta\xi) \\ \vdots & \vdots & \ddots & | & \vdots & \ddots & \vdots \\ \hline O(\delta\xi^{5/4}) & O(\delta\xi^{5/4}) & \cdots & | & 1 & \cdots & O(\delta\xi^{5/4}) \\ \vdots & \vdots & \ddots & | & \vdots & \ddots & \vdots \\ \hline O(\delta\xi) & O(\delta\xi) & \cdots & | & O(\delta\xi^{5/4}) & \cdots & 1 + O(\delta\xi) \end{bmatrix}^{-1} D_0 D_1^{-1} \quad (59)$$

The center block can again be analyzed using the Neumann series. For Bloch wave modes m_B not near transition points, we still have:

$$|T_{L,m_B m_B}| = 1 + O(\delta\xi^2). \quad (60)$$

Direct transmission path

Now we know that the transmittance of the Bloch wave through the Floquet lattice connecting adjacent parameters is $1 + O(\delta\xi^2)$. When a parameter path remains on the Bloch wave, among all scattering paths, there is one corresponding to direct transmission, and its transmittance will be $\lim_{N_s \rightarrow \infty} (1 + O(1/N_s^2))^{N_s} = 1$. As each segment approaches the thermodynamic limit $L_0 \rightarrow \infty$, the Wigner time delay for this path can generally only be physically generated by this path. Therefore, the transmittance of this path serves as a lower bound for the smoothed transmittance, thereby proving that the smoothed transmittance tends to 1.